Appl Phys B (2012) 107:275–283
DOI 10.1007/s00340-012-4949-1

Applied Physics B
Lasers and Optics

Ultra-sensitive carbon monoxide detection by using EC-QCL based quartz-enhanced photoacoustic spectroscopy

L. Dong · R. Lewicki · K. Liu · P.R. Buerki · M.J. Weida · F.K. Tittel

Received: 13 February 2012 / Published online: 21 March 2012
© Springer-Verlag 2012

Abstract A quartz-enhanced photoacoustic spectroscopy (QEPAS) based sensor for carbon monoxide detection at ppbv levels was developed with a 4.65 μm external-cavity quantum cascade laser operating both in continuous wave (cw) and pulsed modes. A 23-fold enhancement of the measured CO signal amplitude was obtained when water vapor, acting as a catalyst for vibrational energy transfer, was added to the targeted analyte mixture. In the cw mode, a noise-equivalent sensitivity (NES, 1σ) of 2 ppbv was achieved at a gas pressure of 100 Torr, for 1-s lock-in amplifier (LIA) time constant (TC), which corresponds to a normalized noise equivalent absorption coefficient (NNEA) of 1.48×10^{-8} cm^{-1} W/$\sqrt{\text{Hz}}$. In the pulsed mode, the determined NES and NNEA were 46 ppbv and 1.07×10^{-8} cm^{-1} W/$\sqrt{\text{Hz}}$, respectively, for a 3-ms LIA TC at atmospheric pressure with a laser scan rate of 18 cm^{-1}/s and a 50 % duty cycle. An intercomparison between cw and pulsed QEPAS-based CO detection is also reported.

1 Introduction

Carbon monoxide (CO) is recognized as a major air pollutant which plays an important role in atmospheric chemistry due to its impact on tropospheric ozone formation [1] and an indirect effect on global warming by reducing the abundance of hydroxyl radicals [2]. The major sources of CO emission into the atmosphere result from the incomplete burning of natural gas and other carbon containing fuels that are widely used for power generation, petrochemical refining as well as automobile and truck transportation. The current method used by the US Environmental Protection Agency for automated and continuous monitoring of ambient CO concentration levels is the nondispersive infrared (NDIR) technique with a typical 1 ppmv detection sensitivity limit, a ∼30 sec response time and sample pretreatment [3]. The availability of a compact CO sensor with ppbv-level detection sensitivity and fast response will allow effective monitoring and quantification of CO urban and industrial emission. Furthermore, CO is also an important cellular signaling molecule [4] next to nitric oxide (NO), since studies have revealed that elevated CO concentration levels in exhaled breath are associated with asthma [5], diabetes [6], and hemolytic diseases [7]. Therefore, ultrasensitive CO detection is also a promising tool for non-invasive medical diagnostics.

Quartz enhanced photoacoustic spectroscopy (QEPAS) since its first demonstration in 2002 has proved to be a sensitive, selective, and noise-immune spectroscopic technique for chemical analysis of gases among available optical methods for trace gas sensing [8, 9]. A compact acoustic detection module (ADM) used in QEPAS based trace gas concentration measurements allows convenient integration with various laser sources and quantification of trace species in small analyzed gas samples (∼3 mm^3) [10]. Another advantage of QEPAS is that it is wavelength independent and is therefore applicable in spectroscopic measurement ranging from the ultraviolet to the mid infrared [11–13]. For laser-based spectroscopic measurements the mid-infrared (mid-IR) region is of special interest because many of the molecular species possess fundamental vibrational absorption bands in this region. Continuous wave (cw) and pulsed quantum cascade lasers (QCLs) whose performance has sig-

L. Dong (✉) · R. Lewicki · K. Liu · F.K. Tittel
Department of Electrical and Computer Engineering,
Rice University, 6100 Main Street, Houston TX 77005, USA
e-mail: lei.dong@rice.edu

P.R. Buerki · M.J. Weida
Daylight Solutions, Inc., 15378 Avenue of Science, San Diego,
CA 92128, USA

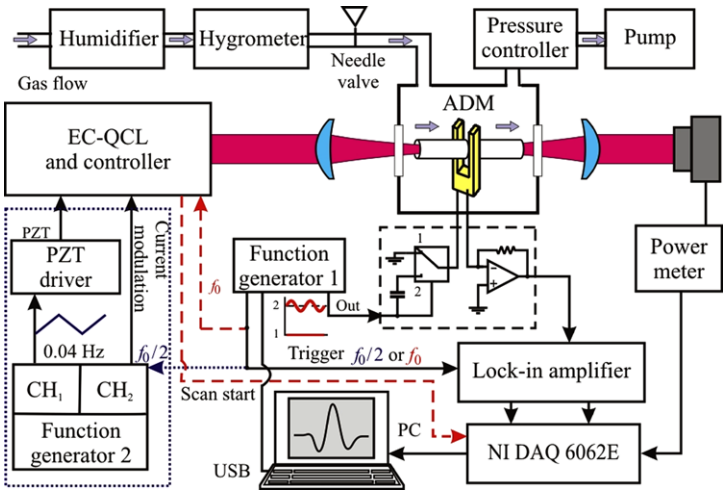

Fig. 1 Schematic of QEPAS based CO sensor

nificantly improved in terms of pulsed and cw output power at room temperature, wall plug efficiency and lifetime in the past 2 years [14, 15] are well-suited QEPAS excitation sources. Therefore, the combination of tunable, single frequency QCL sources and the QEPAS technique has the potential to develop compact, reliable, sensitive, and selective trace gas sensor instrumentation.

This work explores the applicability of QEPAS based CO detection in the mid-IR region. A thermoelectrically cooled, widely tunable, external cavity (EC) QCL at a wavelength of 4.65 μm was employed as the radiation source. The advantages and disadvantages of sensor configuration schemes using both cw and pulsed operation were investigated. Since CO is known to have a slow vibrational-translational (V-T) energy relaxation process, water vapor as a convenient catalyst, produced by a Nafion tube based humidifier, was added to enhance the QEPAS CO signal. This resulted in an EC-QCL based QEPAS CO sensor platform with a ppbv-level detection sensitivity.

2 Description of sensor system

A schematic configuration of the QEPAS based CO sensor is depicted in Fig. 1. A 4.65 μm, tunable thermoelectrically cooled EC-QCL system (Daylight Solutions, Inc., ECqcL™, model #21045) was used as the excitation source operated in either cw or pulsed modes. A water chiller was connected to the laser housing in order to dissipate the heat produced by the thermoelectric cooler of the EC-QCL. The laser temperature and current were controlled by a QCL controller unit and set to 15 °C and 275 mA, respectively. Two 25 mm focal length plano-convex Ge lenses with broadband antireflection (AR) coating were used to focus the laser beam through the ADM and to recollimate the laser radiation upon exiting the ADM. The re-collimated beam was directed to a power meter (Ophir, 3A-SH) for optical power monitoring purposes.

The ADM incorporates a quartz tuning fork (QTF) and two microresonator (mR) tubes inside a compact gas enclosure of total volume of <5 cm^3 [10]. The enclosure consists of an inlet and outlet connection for gas tubes and two 4–12 μm AR coated ZnSe windows attached to the front and back of the enclosure. The QTF was located between the two mR tubes to detect the acoustic waves excited in the gas contained inside the mR. A charge deformation of the QTF prongs due to the piezoelectric effect produces a small current or voltage on electrodes deposited on the QTF surfaces. Subsequently, this QTF electric signal was detected using an ultra-low noise transimpedance preamplifier with a 10 MΩ feedback resistor R_g located close to the ADM. A LabView program was launched to determine critical QTF parameters such as the resonance frequency f_0, Q-factor, and dynamic resistance R, before starting QEPAS measurements. Function generator 1 (Stanford Research System, model DS345), which was controlled by LabView via USB, was employed to output an electrical sine wave excitation voltage with a DC offset. The DC offset opened the electronic switch contained on the preamplifier board to allow excitation of the QTF by the function generator signal. The frequency of the excitation signal was scanned to determine the QTF resonant frequency when measuring the QTF current with a lock-in amplifier (LIA) (Stanford Research, SR830) set to a 1st order harmonic detection mode with respect to the reference frequency. After the scanning was completed, the Q-factor and the dynamic resistance R were calculated based on the complete QTF frequency response profile. Then the output voltage of the function generator 1 was automatically set to 0 V to restore the detection mode of the QTF, while the output frequency was set, as a sync source, either to the $f_0/2$ or f_0 of the QTF resonant frequency.

In the pulsed mode of operation of the EC-QCL based QEPAS sensor, the f_0 sync signal from function generator 1 was delivered to the pulse trigger input of the laser controller

and the external reference input of the LIA. In order to trigger the data acquisition system, a rising-edge scan start signal from the laser controller was employed. These connections are marked with dash lines in Fig. 1. The EC-QCL frequency was continuously scanned bidirectionally over its entire tuning range via the inner ramp generator of the laser controller. However, for analysis purposes, only one direction of spectral data was used. In the cw mode of the EC-QCL based QEPAS sensor, an additional two channel function generator 2 (Tektronix, model AFG3102) was used. The $f_0/2$ sync signal from function generator 1 triggered channel 2 of function generator 2, which produced the same $f_0/2$ frequency sine wave for the current modulation input of the laser housing. The channel 1 of function generator 2 was set to output a 0.4 Hz triangular wave, driving an external PZT driver. These connections and the extra devices were marked on Fig. 1 with a dotted line and dotted box, instead of the dashed lines. The EC-QCL frequency tuning was achieved by applying the output voltage of the external PZT driver to the piezoelectric translator that controls the diffraction grating angle in the EC-QCL housing. The data acquisition system consists of a PC notebook and a National Instruments DAQCard 6062E with which digitization of all the analog signals was performed.

A Nafion humidifier (PermaPure) and a hygrometer (DewMaster, EdgeTech) were connected to the ADM in order to add water vapor to the target gas mixture and monitor its water content, respectively. A needle valve was employed to set the gas flow to a constant rate of 100 scc/min. A pressure controller (MKS Instruments, Inc., Type 640) and an oil free diaphragm vacuum pump were placed after the ADM to control and maintain the CO sensor pressure.

For optimal performance of the QEPAS sensor, it is important to select the geometrical dimensions of the mR tubes, since an appropriate mR configuration can enhance the detection sensitivity up to ~30 times [10]. In addition, the dimensions of the mR tubes have to be adjusted to satisfy the requirements of the EC-QCL based QEPAS CO sensor in both cw and pulsed modes. In the pulsed EC-QCL mode with fast spectral scanning, the slow response time due to the high Q-factor of the QTF can be improved by setting the length of each tube close to half the generated sound wavelength [16]. In this case, the acoustic resonance in the mR is observed with a strongly reduced QTF Q-factor of 1500–2500 at atmospheric pressure. As a result, the response time τ of QTF decreases from ~100 ms to ~20 ms according to the classical oscillator theory $\tau = Q/\pi f_0$. Recent measurements have shown that using a cw EC-QCL source, a half sound wavelength mR tube with 0.84 mm inner diameter can eliminate the undesirable nonzero background caused by the mid-IR QCL beam. A similar detection sensitivity is obtained as with a near-infrared (near-IR) optimal mR tube design at low pressures [17]. Thus, for EC-QCL based CO QEPAS detection using both cw and pulsed modes, two 3.9 mm (half the sound wavelength) long mR tubes with 0.84 mm inner diameter were employed.

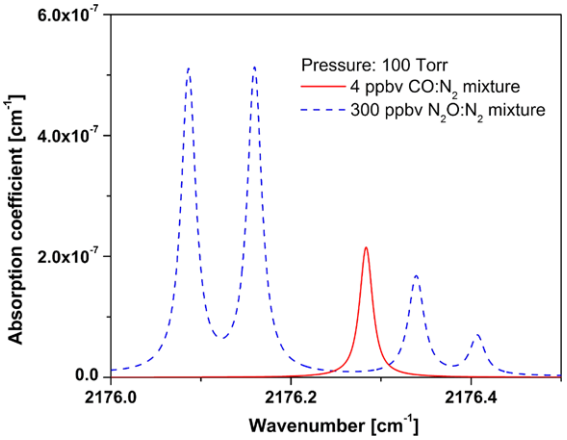

Fig. 2 Simulated CO and N_2O HITRAN spectra. A N_2O interference occurs in the wings of the CO $R(8)$ line at 100 Torr total gas pressure for a gas compositions consisting of 4 ppbv CO, 300 ppbv N_2O, 400 ppbv CO_2, and 2 % H_2O

3 Sensor performance optimization in cw operational mode

Initially, the optical power profile for the 4.65 μm EC-QCL system emitting from 2120 to 2250 cm^{-1} was measured beyond the laser housing. The maximum peak power of 105 mW occurred at 2180 cm^{-1}. The frequency tuning range with an EC-QCL power of >50 mW was observed between 2150 and 2220 cm^{-1}, which partially overlaps with the R branch of the fundamental ro-vibration band of CO centered at 2150 cm^{-1}. Hence, for optimum CO detection, the strongest absorption lines located near the peak of the R branch were investigated. As suitable candidates, two interference-free lines $R(6)$ and $R(8)$ at 2169.20 cm^{-1} and 2176.28 cm^{-1} were identified for environmental monitoring analysis or breath-based medical diagnostics. In this work, $R(8)$ was selected because a more stable EC-QCL operation without mode hopping was achieved at this wavelength. Spectral simulations for environmental monitoring at 100 Torr were performed using the HITRAN 2004 database [18] for H_2O (2 %), CO_2 (400 ppmV), and N_2O (300 ppmV) near the $R(8)$ CO line, as shown in Fig. 2, which indicated only the presence of N_2O as an interference in the analyzed spectral region. When the total gas pressure is >200 Torr, the $R(8)$ line partly overlaps with a weak neighboring N_2O line. Thus, for environmental CO monitoring at the precision limit of single ppbV detection, a low gas pressure condition is required.

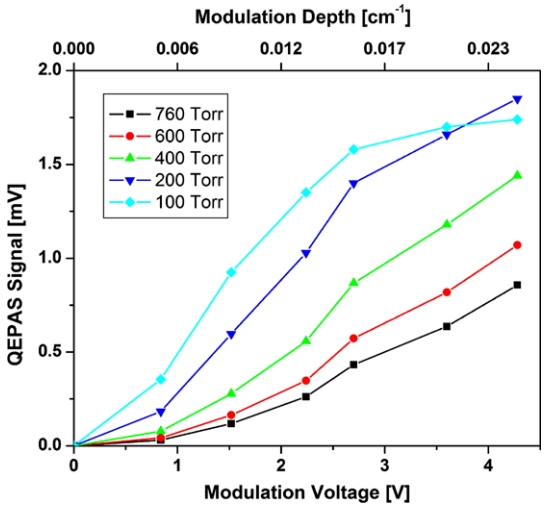

Fig. 3 QEPAS signal corresponding to the peak of the $R(8)$ CO absorption line near 2176.28 cm^{-1} for different laser current modulation depths and gas pressures. A dry 49 ppmv $CO:N_2$ mixture and a 100 SCCM gas mass flow were used

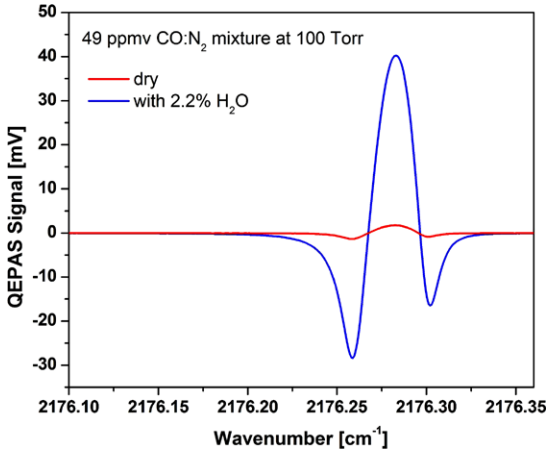

Fig. 4 QEPAS spectra of the $R(8)$ CO absorption line for a dry and a 2.2 % H_2O mixture were acquired with a 49 ppmv CO concentration, 100 Torr total pressure, and a 100 ms lock-in amplifier time constant

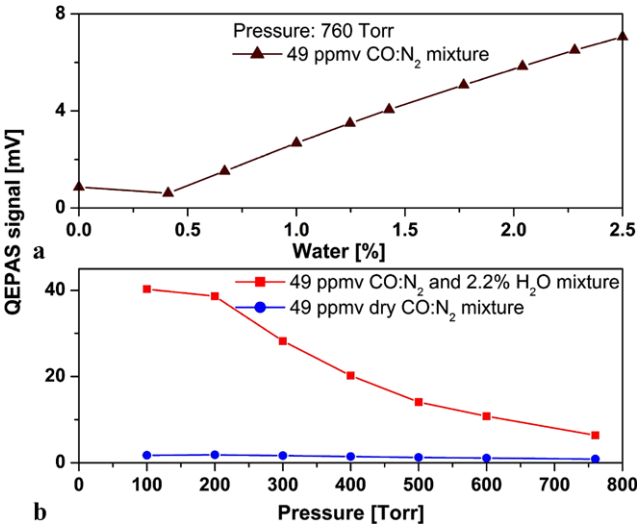

Fig. 5 (a) QEPAS signal obtained from a 49 ppmv $CO:N_2$ mixture at 760 Torr as a function of water concentration. (b) QEPAS signal of a dry 49 ppmv $CO:N_2$ mixture and a 2.2 % H_2O mixture as a function of total gas pressure

The cw QEPAS detection approach is based on $2f$ wavelength-modulation spectroscopy (WMS). The laser modulation depth must match the pressure-dependent absorption linewidth to yield the highest $2f$ signal. Hence, the wavelength modulation depth must be chosen appropriately. The amplitude of the QEPAS signal measured at the peak of the $R(8)$ absorption line as a function of laser current modulation depth and gas pressure was plotted in Fig. 3. The measurements were carried out with a certified mixture of 49 ppmv CO in N_2. Due to the 5 V_{pp} limitation of current modulation voltage the optimal condition for the modulation depth cannot be reached except at a pressure of 100 Torr. Thus, for all QEPAS measurements performed at different pressure conditions a current modulation voltage of 4.3 V_{pp}, corresponding to the amplitude of the modulation depth of 0.025 cm^{-1}, was used.

The signal amplitude depends strongly on the V-T relaxation rate of the target gases in QEPAS based concentration measurements. Water (H_2O) is an efficient catalyst for the vibrational energy transfer reactions in the gas phase. To study the influence of water on promoting the V-T relaxation of the laser-excited vibrational state of CO, 2.2 % of water vapor was added to a certified CO mixture. The CO QEPAS spectra of the $R(8)$ line acquired at 100 Torr for a dry and moisturized 49 ppmv $CO:N_2$ mixture are shown in Fig. 4. The addition of 2.2 % water results in a 23 times signal enhancement, which confirmed that the presence of water can significantly improve CO V-T relaxation rate. Subsequently, the effect of the water present in the CO mixture was investigated by varying its concentration from 0 to 2.5 % by volume at a total gas pressure of 760 Torr. The measured QEPAS signal at the center of the $R(8)$ absorption line as a function of the water concentration is depicted in Fig. 5(a).

For low water concentration levels, a constant level of the QEPAS signal implies that water vapor addition does not provide any improvement for the CO V-T transfer process, until its concentration exceeds 0.5 %. Due to limited performance of the humidifier, the volume percent of the maximum amount of water vapor that can be added to the gas mixture is 2.5 %. However, based on the trend of the curve in Fig. 5(a), the QEPAS signal is expected to reach an optimum level for much higher water vapor concentration than 2.5 %. In fact, such a behavior can be beneficial for breath diagnostic since the water concentration in the exhaled breath is at a ~5 % concentration level. In environmental monitoring, the addition of >2 % water to the analyzed mixture is helpful to improve the CO detection sensitivity.

Another QEPAS parameter that must be optimized is the gas pressure, which strongly influences the QTF Q-factor, molecular V-T transfer time and the enhancement factor of the mR. The CO QEPAS signal amplitude measured at the center of the $R(8)$ absorption line for different gas pressure values are illustrated in Fig. 5(b) for a dry and moisturized (2.2 % water vapor) mixture of 49 ppmv CO in N_2. It was found that using the same water concentration, a ~3 times larger QEPAS signal gain was observed at a low pressure (100 Torr) than at atmospheric pressure. However, for each selected gas pressure, the measured QEPAS system noise level will be different. Therefore, to determine the optimal detection pressure, the signal-to-noise ratio (SNR) should be taken into account. Typically, the QEPAS signal, which consists of both in-phase (X) and quadrature (Y) components, is represented in such a way that the Y component does not contain the photoacoustic signal of CO and, therefore, can be used to evaluate the sensor noise level. From the Y component of the measured QEPAS signal at 100 Torr, the rms noise was measured to be 5.2 μV. The thermal noise of the QTF in each of the two QEPAS signal components can be calculated according to the following equation [8]:

$$\sqrt{\langle V_{\mathrm{N-CW}}^2 \rangle} = \frac{1}{\sqrt{2}} R_{\mathrm{g}} \sqrt{\frac{4k_{\mathrm{B}}T}{R}} \sqrt{\Delta f}, \tag{1}$$

where $T = 297$ K is the temperature, $R = 82.5$ kΩ is the measured equivalent dynamic resistance of the QTF at 100 Torr total pressure, k_B is the Boltzmann constant, and $\Delta f = 2.5$ Hz is the measurement bandwidth (100 ms LIA time constant (TC) with a 12 dB/oct filter slope). The $1/\sqrt{2}$ coefficient reflects the fact that the noise is calculated only for one component. In this case, the rms noise level determined from Eq. (1) is 5.0 μV, which confirms that the measured sensor noise level is at the fundamental thermal noise limit. The SNR was calculated at different gas pressures when 49 ppmv CO in N_2 with the addition of 2.2 % H_2O was passed through the QEPAS system. The maximum SNR value was observed at 200 Torr of gas pressure which is illustrated in Fig. 6. A decrease in the SNR value observed at lower pressures is attributed to the higher noise level caused by the lower values of the QTF dynamic resistance R. For higher pressures, an even steeper decrease in the detected QEPAS signal and, therefore, in the SNR value is observed due to a considerable decrease of the QTF Q-factor. Despite the fact that the 200 Torr pressure was found to be optimal, continuous measurements of the CO concentration level were performed at 100 Torr in order to avoid overlapping between the selected $R(8)$ absorption line of CO and the weak neighboring N_2O line and to obtain the precision of single ppb detection. In this case, the SNR and, therefore, minimum detection limit are ~29 % lower than at the optimum condition.

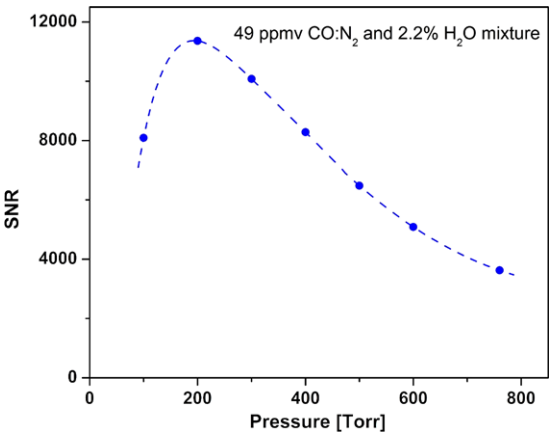

Fig. 6 Signal-to-noise ratio as a function of the total gas pressures for CO detection in a cw operational mode acquired for a 49 ppmv CO:N_2 and 2.2 % H_2O mixture

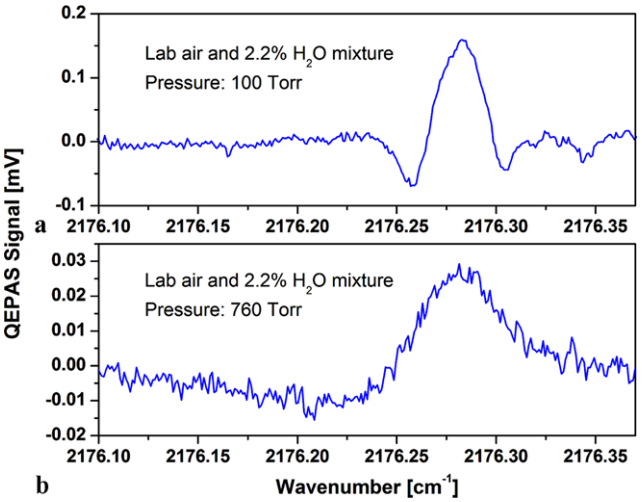

Fig. 7 (**a**) QEPAS spectra of the $R(8)$ CO absorption line acquired at 100 Torr ambient laboratory air. (4.3 V wavelength modulation voltage, 100 ms lock-in amplifier time constant) (**b**) Same spectra with same parameter settings acquired for 760 Torr ambient laboratory air

The $2f$ QEPAS spectrum for an ambient laboratory air concentration of CO is shown in Fig. 7(a). The measurement was carried out at a total gas pressure of 100 Torr, using a 4.3 V_{pp} sine wave current modulation input, and a 35 V_{pp} triangular wave delivered to the piezoelectric transducer and with a 100 ms LIA TC. A constant 2.2 % concentration of water vapor was mixed with sampled laboratory air resulting in a QEPAS signal amplitude of 0.158 mV measured at the center of the CO $R(8)$ line. This signal level, calibrated using a certified mixture of 49 ppmv CO in N_2, corresponds to an ambient CO concentration level of 192 ppbv. In addition, the same CO $R(8)$ absorption line was used in the $2f$ QEPAS measurement of ambient laboratory air at atmospheric pressure. The result of this measurement is shown in Fig. 7(b). The detected QEPAS signal amplitude at the center of the absorption line is 0.026 mV resulting in an am-

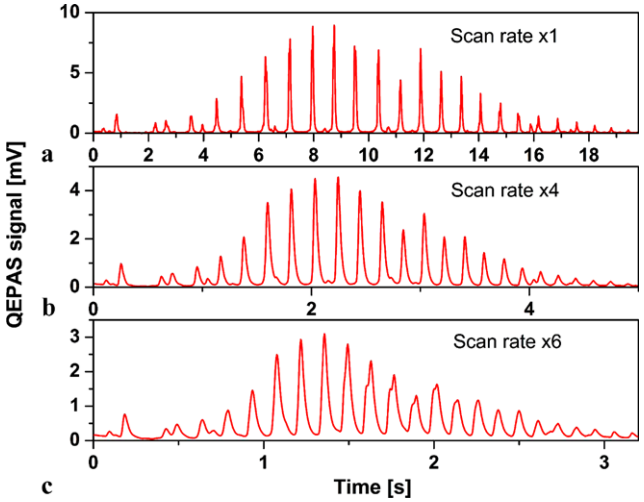

Fig. 8 QEPAS signal of the *R* branch CO absorption line obtained in pulsed operational mode for 49 ppmv CO:N_2 and 2.2 % H_2O mixture and laser wavelength scanning between 2135 cm^{-1} and 2225 cm^{-1}. Three different scan rates, ×1 (**a**), ×4 (**b**), ×6 (**c**) were used

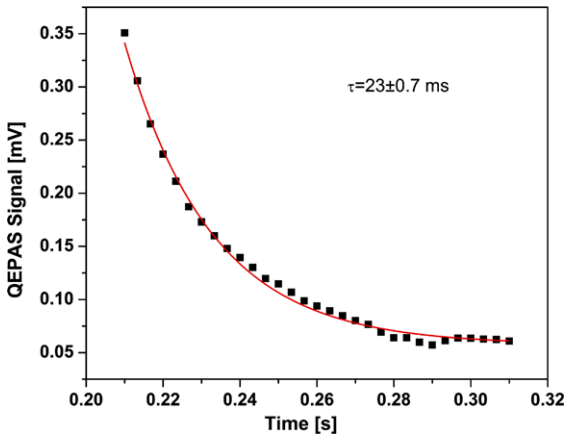

Fig. 9 A 2139.41 cm^{-1} QEPAS based CO absorption line tail (scan rate × 6) and its exponential fit of $e^{-t/\tau}$ where τ is the response time

bient CO concentration level of 200 ppbv. The calculated CO concentration level is in good agreement with the result obtained at a gas pressure of 100 Torr. The difference of 8 ppbV between the two results measured at two different pressures is mainly due to the interference of the N_2O line.

4 Sensor performance optimization in a pulsed operational mode

Sensitive QEPAS measurements of CO concentration levels based on a pulsed operated EC-QCL system were performed using amplitude-modulation spectroscopy (AMS). The LIA was set to the 1st harmonic detection mode with respect to the modulation frequency. To spectrally cover the whole *R* branch of the fundamental ro-vibrational band of CO centered at 4.65 μm, the EC-QCL frequency tuning range was set between 2135 cm^{-1} and 2225 cm^{-1}. The slowest scanning rate, described as "scan rate ×1" by the EC-QCL controller, is 4.5 cm^{-1}/s. The scan rate can be changed in integer multiples up to ×6. The LIA TC and the filter slope were set to 3 ms and 12 dB/oct, respectively. Such an integration parameter setting had been verified to not cause distortion of the spectral lines by the LIA in a previous pulsed QEPAS experiment [16].

Typical spectra of the *R* branch of the fundamental rotational-vibrational band of CO were measured and shown in Fig. 8 when the laser duty cycle was set to 40 %. For three selected scanning rates of ×1, ×4, and ×6, the laser frequency tuning rate was calculated to be 4.5 cm^{-1}/s, 18 cm^{-1}/s, and 27 cm^{-1}/s, respectively. The measurements were carried out at atmospheric pressure using a certified mixture of 49 ppmv CO in N_2 with the addition of 2.2 % water vapor. The best CO *R* branch spectra were acquired for the slowest scan rate ×1 with an acquisition time of ∼20 s. A significant improvement of the acquisition time to ∼3 s can be achieved when the fastest scan rate ×6 was employed. However, the spectra suffered a severe exponentially decaying effect on each line tail due to a comparable QTF response time ($\tau = Q/\pi f$) with the time intervals between subsequent data points (i.e., before the QTF output reached a steady-state value, the laser frequency was adjusted to the next value, which results in overlapping between spectral data points). The tail of the 2139.43 cm^{-1} CO absorption line acquired at scan rate ×6 is shown in Fig. 9. The measured decay time of 23 ± 0.7 ms is in excellent agreement with $\tau = 19$ ms from a theoretical calculation with $Q = 2000$ and $f_0 = 32752$ Hz. In fact, the optimal scan rate should be a compromise between the laser frequency tuning speed and the line shape of the measured spectra. An optimal condition was obtained when the scan rate was set to ×4 (Fig. 8(b)), corresponding to a laser frequency tuning rate of 18 cm^{-1}/s. In this case the exponentially decaying effect is not obvious and the acquisition time required to tune the EC-QCL frequency over the whole *R* branch is only 5 s.

The CO *R* branch spectra recorded in the time domain using scanning rate ×4 (Fig. 8(b)) was transferred into the laser frequency domain by comparing each detected CO absorption line with its representative from the HITRAN spectroscopic database [18]. The calibration curve depicted in Fig. 10(a) shows a quasilinear behavior of the laser frequency tuning with time. The comparison between the frequency-calibrated CO QEPAS spectrum normalized to power (top) and a HITRAN simulated spectrum (bottom) was plotted in Fig. 10(b). The good agreement between experimental and simulation data proves the validity of using the pulsed EC-QCL based QEPAS system for sensitive and high resolution CO measurements.

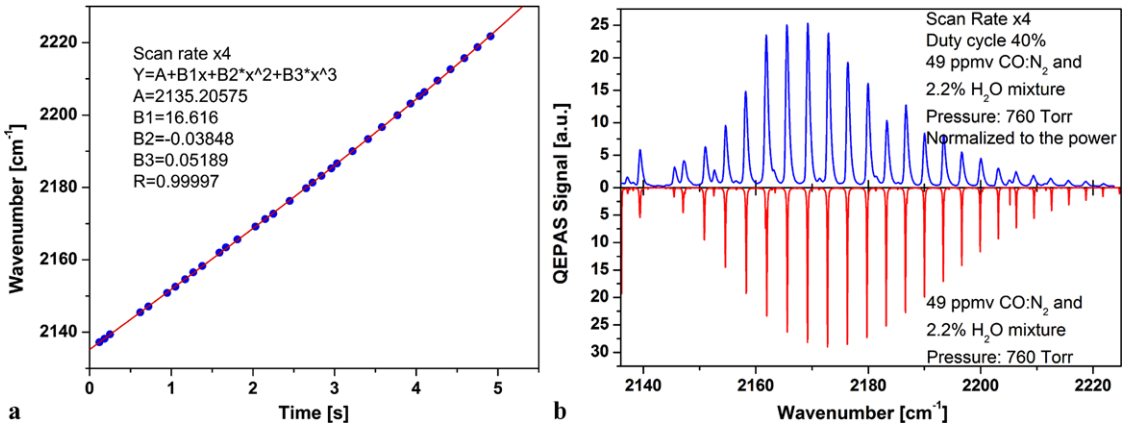

Fig. 10 (**a**) A spectral scan calibration based on data from Fig. 8(b) and the HITRAN database. (**b**) An inter-comparison of QEPAS and HITRAN spectra of the CO R branch at ∼4.65 μm

The LIA TC of 3 ms and filter slope of 12 dB/oct result in an equivalent noise bandwidth (ENBW) of $\Delta f = 83.3$ Hz. This value is much wider than the resonant curve of the QTF calculated as ENBW $= \pi f_0/2Q = 26.4$ Hz. Hence, the QEPAS thermal noise level cannot be calculated using Eq. (1). Instead, the noise power density should be integrated over the resonant curve of the QTF, which is written as [16]:

$$\sqrt{\langle V_{\mathrm{N-P}}^2 \rangle} = \frac{1}{\sqrt{2}} R_{\mathrm{g}} \sqrt{\frac{2\pi k_{\mathrm{B}} T f_0}{RQ}}. \tag{2}$$

For $T = 297$ K, $R = 697.75$ kΩ, $Q = 1947$, and $f_0 = 32752.44$ Hz, the thermal noise was theoretically calculated to be 6.1 μV, while the experimentally measured noise level was ∼10 μV. The higher observed level of noise is caused by QCL radiation that was partially absorbed by the ADM elements and that created an acoustic background at the modulation frequency. Therefore, the QEPAS noise level in a pulsed operation mode is determined by the background rather than by the QTF thermal noise.

For widely tunable QEPAS measurements based on pulsed operated EC-QCL a lower than expected amplitude for several CO absorption lines was observed. This results in a nonuniform envelope of the recorded R branch of CO which probably was due to a laser power change or mode hopping effect. However, scanning across the whole CO R branch with ×4 scan rate and averaging observed QEPAS spectra over 5 times results in <4 % inconsistency when compared to the HITRAN based reference spectrum.

5 Discussions

For the cw QEPAS measurement, the optical laser power at the center of the CO $R(8)$ absorption line was 100 mW. However, the power delivered to the QTF was only 71 mW due to optical losses by the collimating lens and ADM windows. With a LIA TC of 100 ms and a 12 dB/oct filter slope, the ENBW of the sensor is 2.5 Hz. At the gas pressure of 100 Torr, the noise-equivalent sensitivity (NES, 1σ) is 6 ppbv. When normalized to a 1-s LIA TC, the NES (1σ) can be decreased to 2 ppbv. The normalized noise-equivalent absorption coefficient (NNEA) is 1.48×10^{-8} cm^{-1} W/$\sqrt{\mathrm{Hz}}$. The single ppbv-level detection of CO obtained with a cw configured QEPAS sensor is sufficient for use in either environmental or medical diagnostic applications. However, to perform sensitive long term measurements, the CO QEPAS sensor operated in cw mode requires QCL frequency locking, a pressure control system, and a humidifier. A frequency locking system consisting of a reference cell, a photodiode, and a feedback loop, is used to eliminate any laser frequency drift caused by EC-QCL current, temperature or diffraction grating angle variations. A pressure control system and a humidifier are employed to obtain the optimum detection pressure and promote the V-T relaxation rate of CO, respectively.

If measurements are made with the $R(6)$ CO absorption line, the EC-QCL based cw QEPAS measurement can be performed at atmospheric pressure due to the lack of interference from N_2O. Thus, the pressure control system (pressure controller and the vacuum pump) can be removed, which reduces the size and weight of the sensor. Based on the data in Fig. 7(b), the NES (1σ) of CO determined at atmospheric pressure is 13 ppbv with a 100-ms LIA TC. The NES value can be further reduced to 4 ppbv with a 1-s LIA TC, which is only two times worse than those at 100 Torr pressure. The obtained NNEA is 3.52×10^{-8} cm^{-1} W/$\sqrt{\mathrm{Hz}}$. In addition, the humidifier can also be removed when a miniature humidity sensor is used to monitor the water vapor concentration in ambient air. In this case, the detection sensitivity changes with the variation of the water concentration. A correction curve related to wa-

Table 1 Sensitivity for CO:N_2 mixture containing a 2.2 % water vapor by volume. NE—noise equivalent; NNEA—normalized noise-equivalent absorption coefficient

Species	CO:N_2 + 2.2% H_2O		
	CW 100 Torr	CW 760 Torr	Pulsed[a] 760 Torr
LIA TC, s	1	1	0.003
Noise bandwidth, Hz	0.25	0.25	26.4
Laser Power, mW	71	71	7.7
NE sensitivity, ppbv	2	4	123
NE absorption coeff., cm^{-1}	1.04×10^{-7}	2.48×10^{-7}	7.2×10^{-6}
NNEA, $cm^{-1}\,W/\sqrt{Hz}$	1.48×10^{-8}	3.52×10^{-8}	1.07×10^{-8}

[a] duty cycle of 40 % and scan rate × 4; single scan result

ter concentration similar to Fig. 5(a) can be constructed to convert the raw values into the actual concentrations.

The pulsed EC-QCL based QEPAS sensor provides an alternative approach for CO detection. For direct comparison with the cw measurements, the same $R(8)$ absorption line was employed to evaluate the detection sensitivity. The average optical power at the center of the CO $R(8)$ absorption line measured after the ADM was 7.7 mW with 40 % duty cycle. In this case, ∼3 % of the laser radiation was lost when the laser beam was passing through the QTF and mR. The higher noise level, as well as the lower optical power (40 % duty circle), compared to cw mode, resulted in the NES (1σ) of 123 ppbv for LIA TC of 3 ms. This value is not sufficient to monitor atmospheric levels of CO concentration. Normalized to optical power and detection bandwidth, the NNEA is $1.07 \times 10^{-8}\ cm^{-1}\,W/\sqrt{Hz}$. In fact, the worse NES is due to the lower average laser power. With a 50 % duty cycle (the allowed maximum value), the NES (1σ) can be decreased to 46 ppb which, however, is still ∼23 times higher than in the cw QEPAS measurement at low pressure. The measured NNEAs for cw (at 100 and 760 Torr) and pulsed (at 760 Torr) operating mode were summarized in Table 1.

To compare the NNEA for pulsed and cw QEPAS based CO measurements the first term in the Fourier series for the corresponding periodic functions should be taken into account. This yields a correction factor of 3.03 with a 40 % duty cycle from AM-pulses to WM-sine wave [16]. If this factor is involved, the NNEA for pulsed QEPAS measurement corresponds to $3.24 \times 10^{-8}\ cm^{-1}\,W/\sqrt{Hz}$, which is in good agreement with $3.52 \times 10^{-8}\ cm^{-1}\,W/\sqrt{Hz}$ in cw QEPAS measurement at atmospheric pressure.

The QEPAS spectral line width at ×1 scan rate was determined by a convolution of the pressure-broadened absorption line width, the laser line width, and the exponential decay, which was found to be ∼1.5 cm^{-1}, while with the ×4 and ×6 scan rates, the exponentially decaying effect is dominant in the QEPAS spectral line width. Thus, the QEPAS measurements at low pressures are not beneficial to the spectral resolution of the monitored species. It is practical to operate the pulsed EC-QCL based CO sensor at atmospheric pressure without pressure control system. In addition, the locking system is no longer needed since the laser frequency was scanned reproducible across the selected EC-QCL frequency range. This can simplify the system size and weight. Furthermore, pulsed QCLs have a higher wall-plug efficiency and consume less power, allowing future potential to operate with a battery supply. In particular, pulsed EC-QCLs have the capacity for broad tuning, making it possible to detect multichemical analytes simultaneously. For example, with CO detection, water and N_2O concentrations can be analyzed as well.

For recently performed CO measurements using a cw near-IR diode laser based QEPAS sensor platform, a minimum detection sensitivity of 7.74 ppmv was reported [19]. When compared to the detection sensitivity achieved with the mid-IR EC-QCL source, the result is ∼4000 times worse. The significant improvement in the detection limit for EC-QCL based QEPAS sensor is not driven by the different ADM configurations for near and mid-IR regions but is primarily caused by targeting much stronger CO absorption lines in the fundamental mid-IR CO absorption band and by using laser source emitting much higher optical power. In fact, for near-IR diode laser based QEPAS CO sensor, the NNEA coefficient, normalized to the absorption line strength, the optical power, and the detection bandwidth was calculated to be $1.41 \times 10^{-8}\ cm^{-1}\,W/\sqrt{Hz}$ [19]. This value is similar to the one achieved for cw mid-IR EC-QCL based QEPAS CO sensor at 100 Torr, but two times better than the one achieved at atmospheric pressure. The main reason for this is that the geometrical dimensions of the mR in this work were optimized for mid-IR QCL applications [17].

6 Conclusions

This work demonstrates the potential of an EC-QCL based QEPAS sensor for CO detection at ppbv concentration levels using either cw or pulsed operating modes with an optimized acoustic mR configuration. For a cw configured QEPAS CO sensor, a 2 ppbv detection limit for the $R(8)$ CO absorption line was achieved at 100 Torr gas pressure using a 1-s LIA TC. An additional increase in detected QEPAS signal can be addressed by extending maximum current modulation range of the EC-QCL source in order to provide an optimum wavelength modulation depth for WMS measurements of CO. This can be useful at pressures >100 Torr. For pulsed operation mode, a detection sensitivity of 46 ppbv was achieved due to a lower average output power and approximately twice higher, experimentally measured, QEPAS background noise level than the theoretically calculated thermal noise level of the QTF. Hence

this is a promising scheme featuring a simpler configuration for QEPAS applications when integrated with high power pulsed QCLs. Because of the critical role of water vapor on detection improvement of the QEPAS CO signal, either the addition of a fixed water vapor concentration to the system or the continuous monitoring of humidity level is necessary for QEPAS based measurements to precisely determine the concentration of the analyzed CO mixture.

Acknowledgements Daylight Solutions, Inc. and the Rice University Laser Science Group acknowledge the support of a Phase I NASA SBIR Grant No. NNX11CF34P. In addition, the Laser Science Group acknowledges the financial support from a National Science Foundation (NSF) Engineering Research Center subaward for Mid-infrared Technologies for Health and the Environment (MIRTHE) from Princeton University and Grant C-0586 from The Welch Foundation.

References

1. J.A. Logan, M.J. Prather, S.C. Wofsy, M.B. McElroy, J. Geophys. Res. **86**, 7210 (1981)
2. M.A.K. Khalil, R.A. Rasmussen, Science **224**, 54 (1984)
3. United states environmental protection agency, EPA 600/P-99/001F (2000)
4. T.H. Risby, F.K. Tittel, Opt. Eng. **49**, 111123 (2010)
5. K. Zayasu, K. Sekizawa, S. Okinaga, M. YamayA, T. Ohrui, H. Sasaki, Am. J. Respir. Crit. Care Med. **156**, 1140 (1997)
6. P. Paredi, W. Biernacki, F. Invernizzi, S.A. Kharitonov, P.J. Barnes, Chest **116**, 1007 (1999)
7. H. Okuyama, M. Yonetani, Y. Uetani, H. Nakamura, Pediatr. Int. **43**, 329 (2001)
8. A.A. Kosterev, F.K. Tittel, D.V. Serebryakov, A.L. Malinovsky, I.V. Morozov, Rev. Sci. Instrum. **76**, 043105 (2005)
9. A.A. Kosterev, Y.A. Bakhirkin, R.F. Curl, F.K. Tittel, Opt. Lett. **27**, 1902 (2002)
10. L. Dong, A.A. Kosterev, D. Thomazy, F.K. Tittel, Appl. Phys. B **100**, 627 (2010)
11. M. Troccoli, L. Diehl, D.P. Bour, S.W. Corzine, N. Yu, C.H. Wang, M.A. Belkin, G. Höfler, R. Lewicki, G. Wysocki, F.K. Tittel, F. Capasso, J. Lightwave Technol. **26**, 3534 (2008)
12. R.F. Curl, F. Capasso, C. Gmachl, A.A. Kosterev, B. McManus, R. Lewicki, M. Pusharsky, G. Wysocki, F.K. Tittel, Phys. Lett. **487**, 1 (2010)
13. A.A. Kosterev, G. Wysocki, Y.A. Bakhirkin, S. So, R. Lewicki, F.K. Tittel, R.F. Curl, Appl. Phys. B **90**, 165 (2008)
14. A. Lyakh, R. Maulini, A. Tsekoun, R. Go, S. Von der Porten, C. Pfugl, L. Diehl, F. Capasso, C. Kumar , N. Patel, Proc. Natl. Acad. Sci. USA **107**, 18799 (2010)
15. M. Razeghi, Y. Bai, S. Slivken, S.R. Darvish, Opt. Eng. **49**, 111103 (2010)
16. A.A. Kosterev, P.R. Buerki, L. Dong, M. Reed, T. Day, F.K. Tittel, Appl. Phys. B **100**, 173 (2010)
17. L. Dong, V. Spagnolo, R. Lewicki, F.K. Tittel, Opt. Express **19**, 24037 (2011)
18. L.S. Rothman, A. Barbe, C.D. Brenner, L.R. Brown, C. Camy-Peyret, M.R. Carleer, K. Chance, C. Clerbaux, V. Dana, V.M. Devi, A. Fayt, J.M. Flaudi, R.R. Gamache, A. Goldman, D. Jacquemart, K.W. Jucks, W.J. Lafferty, J.Y. Mandin, S.T. Massie, V. Nemtchinov, D.A. Newnham, A. Perrin, C.P. Rinsland, J. Schroeder, K.M. Smith, M.A.H. Smith, K. Tang, R.A. Toth, J. Vander Auwera, P. Varanasi, K. Yoshino, J. Quant. Spectrosc. Radiat. Transf. **82**, 5 (2003)
19. L. Dong, A.A. Kosterev, D. Thomazy, F.K. Tittel, Proc. SPIE **7945**, 50R-1 (2011)